Phonons in submicron ruby films

1991 J. Phys.: Condens. Matter 3 3099

(http://iopscience.iop.org/0953-8984/3/18/005)

J. Phys.: Condens. Matter 3 (1991) 3099–3112. Printed in the UK

Phonons in submicron ruby films

R J van Wijk, J I Dijkhuis and H W de Wijn

Faculty of Physics and Astronomy, Debye Research Institute, University of Utrecht, PO Box 80000, 3508 TA Utrecht, Netherlands

Received 10 December 1990

Abstract. Submicron ruby films of high Cr^{3+} concentration (1 at.%) are used to study the dynamics of phonons in confined geometries. The films, which are grown on sapphire substrates by evaporation and subsequent annealing, are crystalline, and have a well defined c axis collinear with that of the substrate. From the phonon spectrum injected into the substrate by a heater, only resonant 29 cm^{-1} phonons are selected by residual optically excited Cr^{3+} centres in the substrate beneath the film. The part of these 29 cm^{-1} phonons reaching the film is subsequently trapped within the optically excited zone in the film, and their dynamics is studied via the luminescence emanating from $2\bar{A}(^2E)$. In a second experiment, the direct transition between the Zeeman components of $\bar{E}(^2E)$ is studied. In the frequency range of about 1–5 cm^{-1}, the $\bar{E}(^2E)$ system can serve as a tunable phonon detector having submicron spatial resolution.

1. Introduction

In this paper, we study the properties of submicron ruby films grown on sapphire substrates, and investigate how these films can be used to examine acoustic phonons. The interaction of acoustic phonons with optically excited Cr^{3+} in ruby has attracted considerable interest in the past. The interaction permits the generation and detection of the phonons by optical means. Much work has focused on the imprisonment of 29 cm^{-1} phonons resonant with the $2\bar{A}(^2E) - \bar{E}(^2E)$ transition. This so-called phonon bottleneck leads to an elongation, from about 1 ns up to the regime of microseconds, of the effective relaxation time T_{eff} of the spins in equilibrium with the phonons.

The relaxation time T_{eff} is determined, among other things, by the rate at which resonant phonons escape from the excited zone. One mechanism that was found to contribute to the phonon loss is spatial diffusion out of the zone. However, at high excited-ion concentration N^* or large typical zone dimension L, T_{eff} was found to level off, which indicates that mechanisms other than spatial diffusion are more effective under these conditions. Several studies [1–3] have pointed to the involvement of scattering by exchange-coupled Cr^{3+} pairs, which brings about a frequency shift that is large enough to free the phonons from trapping. More specifically, Goossens *et al* [3] suggested that one-site inelastic scattering off weakly exchange-coupled Cr^{3+} pairs is the dominant frequency shifting mechanism. An interesting aspect of this mechanism is that the associated frequency shifts are of the order of the width of the resonant transition, so the mean free path of a frequency-shifted phonon may still be comparable to the zone dimension. As a result, the efficiency of the mechanism

0953-8984/91/183099+14$03.50

depends not only on N^*, but, as in the case of spatial diffusion, also on L. In fact, if N^* is much larger than the number of resonant phonon modes, the product N^*L is the parameter determining the effective relaxation time in both phonon loss mechanisms.

The complementary role of N^* and L was demonstrated for zone dimensions varying by an order of magnitude upwards from 60 μm [3]. In the work discussed here, the typical zone dimension is reduced to submicron size. In a separate paper it was shown that zones of these dimensions can be created in bulk ruby crystals by the use of the evanescent field of an optical waveguide [4]. In the present work, submicron ruby films grown on sapphire substrates are used to create zones of reduced dimension by conventional optical pumping.

Another extensively studied resonant interaction between optically excited Cr^{3+} ions in ruby and acoustic phonons is direct spin–lattice relaxation between the Zeeman components of the metastable $\bar{E}(^2E)$ Kramers doublet. Firstly, the $\bar{E}(^2E)$ doublet was used to observe excited-state electron spin resonance [5]. Secondly, it constituted an ideal system for testing the dependence of direct spin–lattice relaxation on the magnitude and orientation of magnetic fields [6]. This culminated in the use of the Kramers doublet as a tunable frequency-selective generator and detector of phonons in the frequency range of, say, 1–15 cm^{-1}. And, thirdly, the transition was used to observe phonon amplification through stimulated emission following population inversion brought about by selective optical pumping into the upper level [7]. In this paper we consider the direct relaxation within the magnetic-field split $\bar{E}(^2E)$ doublet of Cr^{3+} in submicron ruby films. Due to the well defined orientation of the crystal lattice in the ruby film, the relaxation shows essentially the same dependences on the magnetic field as in the bulk. This makes it possible to use submicron ruby films as tunable phonon detectors achieving exceptional spatial resolution in the frequency range 1–5 cm^{-1}.

2. Sample preparation and characteristics

The samples used consisted of submicron ruby films of high ($\sim$ 1 at.%) Cr^{3+} content on sapphire substrates. The substrates measured $10 \times 10 \times 0.4$ mm^3, with the c axis oriented parallel to the larger faces. The latter were optically polished, and the ruby layers were subsequently deposited on to the central part of one of these faces by evaporation of ground 1 at.% ruby at a temperature of 2200 °C. The deposited material showed a brownish hue, which disappeared after subsequent annealing in air for 12 hours at about 1500 °C. The film thickness, measured by a scanning-needle instrument, typically ranged from 0.5 to 0.7 μm.

The R_1 luminescent lines emanating from the films were found to be broadened to 0.6 cm^{-1} at 1.8 K. Integrated over the frequency, they are about 70 times more intense than the R_1 emission from the sapphire substrate, which at the given Cr^{3+} concentration in the film of 1 at.% implies a residual Cr^{3+} concentration in the substrate of the order of 0.2 at.ppm. Estimates from Cr^{3+} pair spectra (figure 1) confirm that the Cr^{3+} concentration is indeed of order 1 at.%. In a magnetic field, the R_1 lines of film and substrate show identical Zeeman splittings (figure 2). Since the g factor of $\bar{E}(^2E)$ in ruby is strongly dependent on the direction of the magnetic field relative to the c axis ($g_\parallel = 2.445$ [5] and $g_\perp = 0.05$ [8], while $g = 1.98$ for the $^4A_2$ ground state), this indicates that the ruby films possess a unique c axis that is collinear with that of the substrate. Apparently, they have crystallized with perfect adaptation to

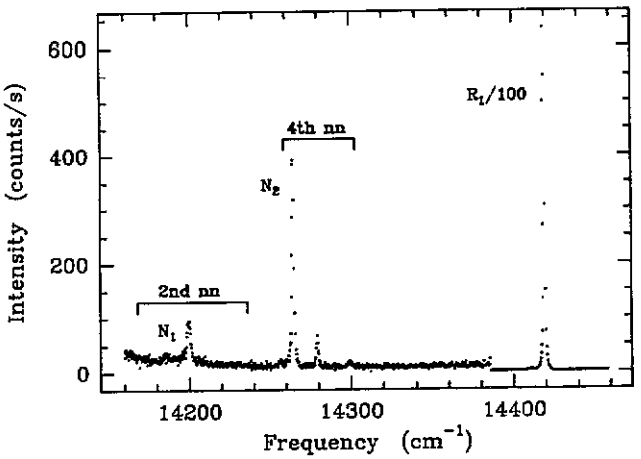

Figure 1. Portion of the luminescence spectrum at 1.8 K, showing the N_1 second-nearest neighbour lines, the N_2 fourth-nearest neighbour lines and the R_1 lines. The detection sensitivity was reduced by 100 around the R_1 line.

the sapphire crystal lattice. No significant further broadening of the R_1 transitions was observed upon applying magnetic fields up to 6 T at large angles ($\sim 70°$) to the c axis. This poses an upper limit of 0.3° on any mosaic spread.

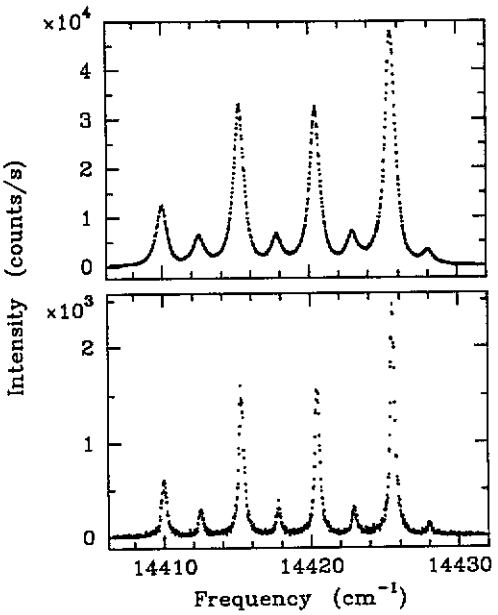

Figure 2. The R_1 luminescence from the ruby film (top) and the substrate (bottom) at $\theta = 67.3°$ in a field of 5.6 T. Temperature is 1.8 K. Instrumental resolution is 0.2 cm^{-1}.

3. Bottlenecking of 29 cm^{-1} phonons

3.1. Dependence of the relaxation on excited-ion concentration

In the experiments the sample was immersed in liquid helium pumped down to a temperature of 1.8 K. A high concentration of excited Cr^{3+} ions was maintained in the film by optical pumping via the broad bands with the focused beam of an Ar ion laser operating at all lines (figure 3). An acousto-optical modulator periodically interrupted the pumping at a rate of 2 kHz, which is sufficiently fast for the pumping to be quasi-stationary. In the absence of optical pumping, i.e. when higher-order processes like Raman relaxation induced by zone-boundary phonons have died out, a constantan heater, deposited on to the ruby film at a distance of about 1 mm from the excited zone, was repetitively fired to produce the phonons at a rate of order 10^5 Hz. The luminescence emanating from the sample was detected at right angles to the laser beam. The sample was held at an angle such that the laser beam and the optical detection system had access to the ruby film from above. The collected R_2 luminescence probing the phonons was detected by means of a 0.85 m double monochromator followed by standard photon counting, and its temporal development was analysed by the use of a time-to-amplitude converter in conjunction with pulse-height analysis.

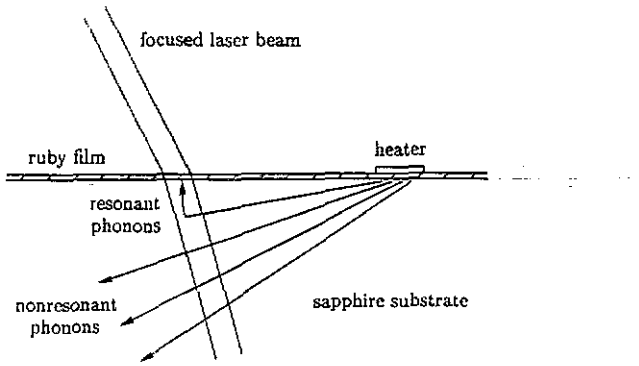

Figure 3. Schematic representation of the experimental geometry.

The decay of the R_2 luminescence following a heat pulse can, within the error bars, be described by a single exponential. The resultant effective decay time T_{eff} after a heat pulse of 1 μs duration, shown in figure 4 as a function of N^*, turns out to be about 200 ns and only marginally dependent on N^*. The near independence of T_{eff} on N^* resembles the levelling off of T_{eff} which is generally found in ruby at high N^*, and which can be explained by the mechanism of one-site spectral wipe-out by weakly exchange-coupled Cr^{3+} pairs. A final value of the order of 200 ns in 1 at.% ruby is indeed expected from extrapolation of the values found for high N^* in 700 at.ppm ruby ($\sim$ 1.2 μs) and 2500 at.ppm ruby ($\sim$ 0.6 μs) in [3].

An adjustment to the data of the expression for T_{eff} derived in the model for spectral wipe-out (cf [3, 4]) is also shown in figure 4, and seen to yield a satisfactory description of the data. Here, we have adopted the more refined criterion for the mean free path in relation to the flight path towards the crystal boundary derived in [4]. This criterion distinguishes between frequency shifts large enough to result in wipe-out and

shifts not resulting in wipe-out. In the present case, however, the precise choice of the criterion has no significant effects on the predictions of the model. The model contains only one adjustable parameter, namely the measure α for the broadening of the phonon transition with increasing exchange. Unfortunately, an accurate determination of α is hampered by the uncertainty in the width $\Delta\nu$ of the $2\bar{A}(^2E) - \bar{E}(^2E)$ transition in 1 at.% ruby. Linear extrapolation of the widths measured earlier by fluorescence line narrowing in 700 and 2500 at.ppm ruby [9] only provides an estimate of the order of 0.1 cm^{-1}. Spatial diffusion towards the zone border as a mechanism of phonon removal, which would make a contribution to T_{eff} that is quadratically dependent on N^*, is apparently insignificant. This suggests that the value $\Delta\nu \sim 0.1$ cm^{-1} is an upper limit. A lower limit is, of course, set by the value of 0.04 cm^{-1} found in 2500 at.ppm ruby. As it turns out, with values of $\Delta\nu$ in the range 0.04–0.1 cm^{-1} the model satisfactorily accounts for the data with $\alpha = 0.08$.

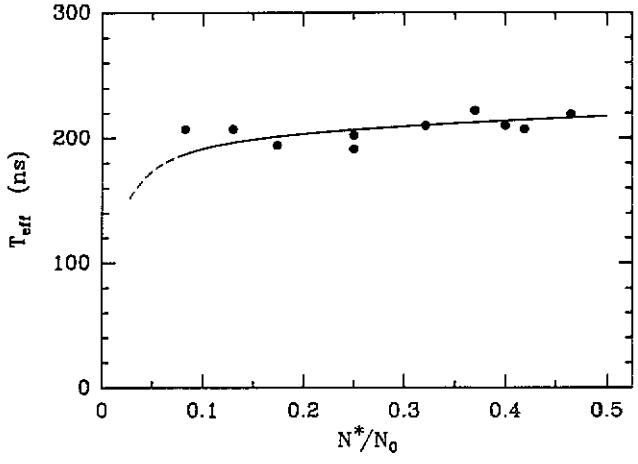

Figure 4. Decay time of $2\bar{A}(^2E)$ after heat pulses of 1 μs duration plotted against the excited-ion concentration N^*, expressed as a fraction of the total Cr^{3+} concentration $N_0 = 4.3 \times 10^{20}$ cm^{-3}. The curve represents the decay time according to spectral wipe-out with $\Delta\nu = 0.06$ cm^{-1} and $\alpha = 0.08$.

3.2. Dependence of the relaxation on heat-pulse duration

Quite remarkably, T_{eff} is found to be affected by the duration of the heat pulse. Shorter heat pulses result in an increasingly pronounced decrease of T_{eff}. This is shown in figure 5, where T_{eff} is plotted against the duration T_h of the build-up of the R_2 luminescence. In all cases, this build-up was somewhat longer (typically 50 ns) than the duration of the electrical pulse applied to the heater.

To discuss this behaviour, we consider the mechanism by which phonons are fed into the excited zone. We first note that the phonons emitted by the heater primarily spread out into the sapphire substrate (figure 3). Since the heater is positioned at about 1 mm from the excited zone, direct propagation along the ruby film is negligible. In the substrate, the phonons travel by ballistic flight, except in the region just below the excited part of the film. In this region, residual Cr^{3+} ions have been excited by the focused laser light traversing the sapphire substrate. The typical N^* amounts to

only $\sim 2 \times 10^{15}$ cm^{-3}, but this is enough to reduce the mean free path of 29 cm^{-1} phonons against resonant scattering to a distance of order 40 μm. Within the laser beam, therefore, the resonant phonons engage in a diffusive motion, and some of them ultimately reach the substrate–film interface. In other words, the heat pulse indirectly supplies from below a more-or-less constant population of resonant phonons at the interface. It is interesting to note that these phonons are virtually *monochromatic* because the line width of the $2\bar{A}(^2\mathrm{E}) - \bar{E}(^2\mathrm{E})$ transition in sapphire approximates the homogeneous width of the transition ($\Delta\nu = 0.008$ cm^{-1} [9]).

Feeding of 29 cm^{-1} phonons into the excited zone by this mechanism does indeed account for the dependence of T_{eff} on the pulse duration. The crucial point is that the decay following termination of the phonon supply at the interface depends on the depth to which the phonons have progressed into the film within the duration of the heat pulse. During the heat pulse, resonant phonons penetrate into the film by spatial diffusion, where their mean free path Λ is reduced to a few nanometres. However, as soon as the phonon population maintained at the substrate–film interface has disappeared at the end of the heat pulse, the diffusive motion in part reverses direction, moving towards the substrate. For heat pulses of short duration, the majority of the phonons return to the substrate. The smaller the penetration depth at the moment the phonon supply ceases, the faster the phonons return. For long durations of feeding, on the other hand, a substantial number of phonons have penetrated into the film to such a depth that they cannot make it to the substrate by spatial diffusion within their resonant lifetime. The latter, determined by spectral wipe-out, then limits the decay time, rendering it independent of the heat-pulse duration.

To explore this further, we rely on a model calculation that is admittedly crude as far as phonon decay by frequency shifting mechanisms is concerned, but has the virtue of being analytical. It incorporates the diffusive motion from and to the interface as well as the essential ingredient of a non-diffusive decay, and in this way yields a more quantitative explanation of the data of figure 5. The starting point is the set of phenomenological rate equations for the concentration $N_{2\bar{A}}$ of Cr^{3+} ions in the $2\bar{A}(^2\mathrm{E})$ level and the occupation number p of the resonant phonons. For any distance z from the film–substrate interface, these equations can be written

$$\frac{\partial N_{2\bar{A}}}{\partial t} = -\frac{(1+p)N_{2\bar{A}} - pN_{\bar{E}}}{T_{\mathrm{d}}} \tag{1a}$$

$$\rho\Delta\nu\frac{\partial p}{\partial t} = \frac{(1+p)N_{2\bar{A}} - pN_{\bar{E}}}{T_{\mathrm{d}}} + \rho\Delta\nu D_{\mathrm{p}}\frac{\partial^2 p}{\partial z^2} - \rho\Delta\nu\frac{p}{\tau_{\mathrm{p}}} \tag{1b}$$

in which T_{d} is the $2\bar{A}(^2\mathrm{E}) - \bar{E}(^2\mathrm{E})$ transition time, $N_{\bar{E}}$ the concentration of Cr^{3+} ions in the $\bar{E}(^2\mathrm{E})$ level, and $\rho\Delta\nu$ is the density of resonant phonon modes. The quantity D_{p} is the phonon diffusion constant, which equals $\frac{1}{3}\Lambda v$, where v is the velocity of sound. Phonon loss has been incorporated parametrically through the constant probability $1/\tau_{\mathrm{p}}$ that the phonon will end its resonant life without return to resonance, such as by spectral wipe-out. Note that τ_{p} depends on N^*. Radiative decay to the $^4\mathrm{A}_2$ ground state has been neglected as it is orders of magnitude slower ($\tau_{\mathrm{R}} \sim 4$ ms) than the timescale of our experiments.

We proceed by noting that the Cr^{3+} spins and the resonant phonons are in dynamic equilibrium, i.e. $N_{2\bar{A}} = [p/(1+p)]N_{\bar{E}} \approx pN^*$. After summing equations (1*a*) and (1*b*) to eliminate the fast dynamic terms connecting phonons and spins, and inserting this

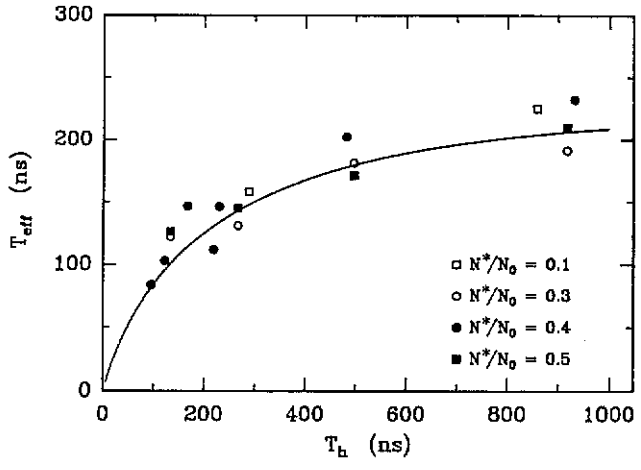

Figure 5. The decay time of $2\bar{A}(^2\mathrm{E})$ after termination of the heat pulse plotted against the duration T_h of the build-up of the R_2 luminescence. Entries resulted from fits to a single-exponential. The curve is explained in the text.

$N_{2\bar{A}}$, the differential equation for p becomes

$$\frac{\mathrm{d}p}{\mathrm{d}t} = D_{2\bar{A}} \frac{\partial^2 p}{\partial z^2} - \frac{p}{T_p}. \tag{2}$$

Here, the quantities $D_{2\bar{A}}$ and T_p, defined by

$$D_{2\bar{A}} = \frac{D_p}{N^*/\rho\Delta\nu + 1} \tag{3}$$

$$T_p = (N^*/\rho\Delta\nu + 1)\tau_p \tag{4}$$

incorporate the coupling of the phonons to the spin system.

The build-up of the phonon population in the film after the start of the heat pulse is derived by solving equation (2) under the condition that the initial p vanishes everywhere in the film, except at $z = 0$, where a constant phonon occupation p_0 is maintained at all times. If the finite film thickness is neglected, the solution for $t > 0$ is [10]

$$p_{in}(z,t) = \tfrac{1}{2}p_0\left[\exp(-z/\zeta)\,\mathrm{erfc}\left(z/2\sqrt{D_{2\bar{A}}t} - \sqrt{t/T_p}\right)\right.$$
$$\left. + \exp(+z/\zeta)\,\mathrm{erfc}\left(z/2\sqrt{D_{2\bar{A}}t} + \sqrt{t/T_p}\right)\right] \tag{5}$$

in which $\zeta = \sqrt{D_{2\bar{A}}T_p}$, and erfc denotes the complementary error function.

Let us consider the distribution of the phonon occupation number over the zone generated during the heat pulse. At long times in comparison with the resonant life time T_p, equation (5) reduces to the time-independent distribution

$$p_\infty(z) = p_0 \exp(-z/\zeta) \tag{6}$$

so ζ, which typically is less than 100 nm, may be interpreted as an effective penetration depth. This implies that according to the model the phonons penetrate into the film

over a distance which is only a fraction of its submicron thickness. For short heat pulses, the phonons penetrate even less deeply, and the exponential distribution is not achieved. The limited penetration warrants our neglect of the finite film thickness in deriving equation (5).

In order to find an expression for the decay of the phonon population in the excited zone after termination of the heat pulse at a time T_h, we solve equation (2) with the initial distribution $p_{in}(z, T_h)$, except that p is assumed to vanish at $z = 0$ at all times. By simple considerations it can be verified that these conditions are satisfied by the solution ($t > T_h$)

$$p_{out}(z,t) = p_{in}(z,t) - p_{in}(z, t - T_h). \tag{7}$$

The R_2 luminescence measured in the experiments is proportional to the phonon population integrated over the excited zone, $\bar{p}$. Integration of equations (5) and (7) yields

$$\bar{p}(t) = p_0\zeta[1 - \mathrm{erfc}(\sqrt{t/T_p})] \qquad 0 < t < T_h \tag{8a}$$

$$\bar{p}(t) = p_0\zeta[\mathrm{erfc}(\sqrt{(t - T_h)/T_p}) - \mathrm{erfc}(\sqrt{t/T_p})] \qquad T_h < t. \tag{8b}$$

Note that ζ only affects the intensity of the luminescence, whereas T_h in relation to T_p determines its development with time.

Equation (8*b*) does indeed predict a faster decay for short heat pulses. A problem remaining when the comparison is made quantitative, however, is that equation (8*b*) yields decays that, strictly speaking, are markedly non-exponential. In particular, the initial decay is too abrupt in comparison with the experiment. The predictions of the model over somewhat longer times after the heat pulse give a faithful description of the complete experimental decay of the R_2 luminescence. The differences between model and data can be understood from two major approximations made in the model. The first is the assumption that the phonon population at the substrate–film interface disappears instantaneously, whereas in reality at least ~ 50 ns are needed. Secondly, phonon frequency shifts that are too small to provide spectral wipe-out but markedly increase the phonon mean free path are neglected. This results in an overestimate of the confinement of the phonons to the film–substrate interface. Phonons with an appreciable frequency shift, in fact, will be distributed more evenly over the film, which will lead to a predominantly exponential decay of their population.

In order to compare T_{eff} in figure 5 with the model, we have calculated the time at which $\bar{p}$ according to equation (8*b*) has dropped to 1/e of its initial value. The results are shown in figure 5 as the full curve, which accurately tracks the data. We note that the choice of the criterion 1/e has, within reasonable limits, only minor effects on the shape of the curve, yet significantly affects the value of T_{eff} reached at large T_h. The adjusted value of $T_p = 0.5$ μs, in fact, is significantly larger than the time for wipe-out estimated directly from the data at large T_h (cf figure 4). Removal of the simplifying assumptions from the model indeed tends to reduce T_p. The disparity, therefore, does not seem to detract from the conclusion that the mechanism of the feeding of resonant phonons via the substrate to the excited zone causes T_{eff} to depend on the duration of the heat pulse.

4. Relaxation within the $\bar{E}(^2E)$ doublet

In this section the relaxation between the $\bar{E}(^2E)$ Zeeman components of Cr^{3+} in a submicron ruby film is examined. The significant distinctions from the situation in the

bulk are the reduced dimension and the associated fast removal of phonons. When the $\bar{E}(^2\mathrm{E})$ system is used as a detector, the reduced dimension greatly enhances the spatial resolution. Furthermore, the variation of the response time due to imprisonment of the resonant phonons is minimized.

4.1. Direct relaxation within $\bar{E}(^2\mathrm{E})$ in a magnetic field

In a magnetic field the $\bar{E}(^2\mathrm{E})$ Kramers doublet is split into its Zeeman components with an energy splitting δ, which is determined almost entirely by the field component parallel to the c axis. This is due to the high anisotropy of the g factor, which equals $g_{\parallel} = 2.445$ for fields parallel to the c axis [5], but amounts to only $g_{\perp} = 0.05$ for perpendicular fields [8]. Thus $\delta \approx g_{\parallel}\mu_{\mathrm{B}} H \cos\theta$, where θ is the angle between the field and the c axis, and H is the field strength.

The direct spin–lattice relaxation between the Zeeman components of $\bar{E}(^2\mathrm{E})$ has been treated theoretically by Blume *et al* [11]. They pointed out that, because $\bar{E}(^2\mathrm{E})$ is a Kramers doublet, direct phonon-assisted transitions are not allowed unless another appropriate Kramers doublet is mixed in by the magnetic field. In the case of $\bar{E}(^2\mathrm{E})$, the admixed Kramers doublet is $2\bar{A}(^2\mathrm{E})$. The admixing and the resulting matrix element connecting the $\bar{E}(^2\mathrm{E})$ Zeeman levels result principally from the magnetic field perpendicular to the c axis, $H\sin\theta$. The characteristic time $T_{\bar{E},\mathrm{d}}$ associated with the direct spin–lattice relaxation is thus found to satisfy

$$\frac{1}{T_{\bar{E},\mathrm{d}}} = CH^5 \cos^3\theta \sin^2\theta \coth\left(\frac{\delta}{2k_{\mathrm{B}}T_0}\right) \tag{9}$$

in which T_0 is the crystal temperature, and C is a constant including, among other things, the spin–lattice interaction. In addition to the relevant matrix element squared, which yield a factor $(H\sin\theta)^2$, equation (9) contains the level separation energy $\delta \propto H\cos\theta$ and a factor $(H\cos\theta)^2$ accounting for the density of the resonant phonon modes, which in the Debye approximation scales with δ^2. The factor $\coth(\delta/2k_{\mathrm{B}}T_0) = 1 + 2p_0$ accounts for the finite phonon occupation number p_0 at finite temperatures.

The direct relaxation within $\bar{E}(^2\mathrm{E})$ can be examined experimentally by populating the $\bar{E}(^2\mathrm{E})$ levels in a ratio that deviates from thermal equilibrium, and subsequently detecting the temporal development of the R_1 luminescence of either of the Zeeman components. The ratio of the level populations returns to its value at thermal equilibrium with time constant $T_{\bar{E},\mathrm{d}}$. This development is superimposed on the radiative decay to the $^4\mathrm{A}_2$ ground state (radiative decay time $\tau_{\mathrm{R}} \sim 4$ ms), to which both levels are subject. In an experiment of this kind in 700 at.ppm ruby [6], equation (9) was found to be in excellent agreement with the measured direct relaxation rates. The constant C was found to be 47 $\mathrm{T}^{-5}\,\mathrm{s}^{-1}$, compared to a predicted value of 27 $\mathrm{T}^{-5}\,\mathrm{s}^{-1}$. To give an indication of the magnitude of $T_{\bar{E},\mathrm{d}}$, we adopt the experimental value of C and take $\theta = 39°$, i.e. the angle for which the relaxation rate is largest for a given H and T_0. At 2 K, then, $T_{\bar{E},\mathrm{d}} = 14$ μs for $H = 6$ T, increasing to τ_{R} for $H = 1.4$ T.

We note that the Zeeman levels of $\bar{E}(^2\mathrm{E})$ are not only connected by direct relaxation, but also by Raman relaxation and resonant Raman relaxation via $2\bar{A}(^2\mathrm{E})$. The latter process, also known as Orbach relaxation, is the most efficient. At 4.2 K, resonant Raman relaxation has a characteristic time of the order of nanoseconds [5]. However, because of its dependence on the number of resonant 29 cm^{-1} phonons present, its efficiency decreases exponentially with temperature, leading to relaxation times of the order of seconds at the temperatures at which our experiments were carried out.

4.2. Experimental details

In the experiments, the sample was immersed in liquid helium pumped down below the λ point to a temperature of 1.8 K. A superconducting magnet in the optical cryostat supplied magnetic fields of up to 6.5 T. An argon ion laser optically pumped Cr^{3+} to $\bar{E}(^2E)$ via the broad bands. With the beam focused to a spot of ~ 100 μm diameter, a laser power of typically 2 W resulted in the rather high $N^* \approx 10^{20}$ cm^{-3} necessary to obtain sufficient R_1 luminescence intensity. The detection differed from the experiment in section 3 in that the time-to-amplitude conversion was replaced by a multichannel scaler with a minimum channel time of 1.2 μs. The experiment tracked the time development of the population of the upper $\bar{E}(^2E)$ level via one of the four R_1 Zeeman components. To this end, the exciting laser beam was repetitively interrupted with the acousto-optical modulator at a frequency of 0.2 kHz and a duty cycle of 50%. Further, the complete R_1 emission spectrum was measured for every run by slow synchronous scanning of the monochromator and the multichannel analyser. Subsequent analysis of the Zeeman splitting of these spectra allowed a precise in-situ determination of the magnetic field inclusive of its orientation relative to the c axis.

Under the conditions of the experiments, interruption of the optical pumping leaves the populations of the $\bar{E}(^2E)$ levels in a ratio close to that of thermal equilibrium. In disturbing this population ratio, we again relied on heat pulses applied in the absence of optical pumping. To obtain a sufficient population difference, it was necessary for these pulses to last for about 4 μs, which is an order of magnitude shorter than the direct $\bar{E}(^2E)$ relaxation time, but substantially longer than the relaxation time associated with the $2\bar{A}(^2E) - \bar{E}(^2E)$ transition. The most likely process causing the redistribution over the populations within $\bar{E}(^2E)$, therefore, is Orbach relaxation via $2\bar{A}(^2E)$ [5]. The fact that the heat pulse duration needed is substantially longer than the typical relaxation times associated with this process is consistent with the conclusion reached in the previous section with regard to the dynamics of 29 cm^{-1} phonons. The long heat-pulse duration allows the 29 cm^{-1} phonons to penetrate the entire excited zone, and to disturb the $\bar{E}(^2E)$ population ratio everywhere.

To extract the $\bar{E}(^2E)$ inter-level relaxation time from the time-resolved spectra, the radiative return back to $^4A_2$ was removed by fitting the expression

$$N_+(t) = [A_1 \exp(-t/T_{\bar{E}}) + A_2] \exp(-t/\tau_R). \tag{10}$$

Here, the decay time τ_R of the R_1 luminescence was fixed at the value measured separately by observing the decay of R_1 in zero field. The result $\tau_R = 3.52$ ms is slightly smaller than the bulk τ_R in, say, 0.1 at.% ruby, presumably because of the higher Cr^{3+} concentration and the absence of reabsorption of R_1 light. The results for $T_{\bar{E}}$ are shown as a function of H and θ in figures 6 and 7 respectively. The ranges of H and θ that could be covered in these experiments are smaller than in the bulk [6], because the increased width of the various components of the R_1 line extends the regions in which they substantially overlap. In measuring the H dependence, we chose θ close to 66°, where the splitting of the $\bar{E}(^2E)$ level is half of that of the ground state, yielding an optimal separation between adjacent R_1 lines emanating from different $\bar{E}(^2E)$ Zeeman levels. The data in figure 7 agree well with equation (9). However, for a complete description of the data it is mandatory to consider the effects of residual trapping of the phonons resonant with the transition.

4.3. Bottlenecking of the direct relaxation

Trapping of phonons resonant with the direct transition can result in an apparent

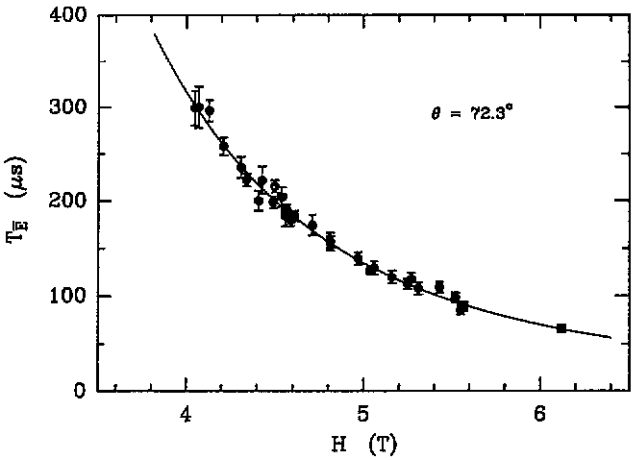

Figure 6. The direct relaxation time between the Zeeman components of $\bar{E}(^2\mathrm{E})$ plotted against the magnitude of the magnetic field H. The angle between the magnetic field and the c axis θ is 72.3°. The curve is a fit of equation (17) to the data.

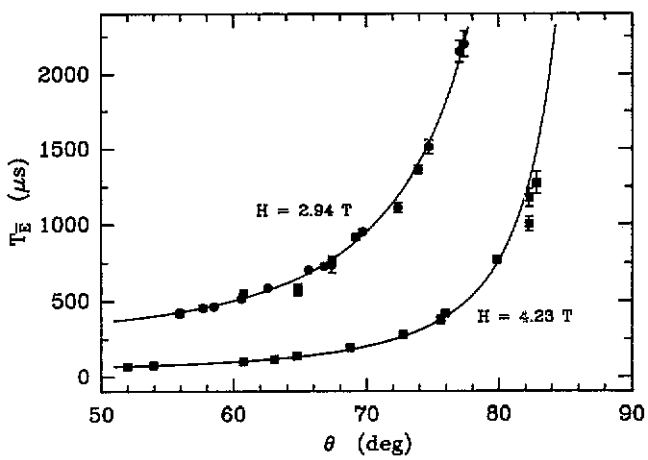

Figure 7. The direct relaxation time within $\bar{E}(^2\mathrm{E})$ plotted against the angle θ between the magnetic field and the c axis for $H = 2.94$ and 4.23 T. The curves are fits of equation (17) to the data.

increase of the direct relaxation time. In our experiments, the bottlenecking turns out to be small, but not negligible. To estimate the effects we consider the rate equations for the decay of the populations N_+ and N_- of the upper and lower $\bar{E}(^2\mathrm{E})$ levels, respectively, and the occupation number p of the resonant phonons. That is

$$\frac{\mathrm{d}N_+}{\mathrm{d}t} = -\frac{(1+p)N_+}{T_s} + \frac{pN_-}{T_s} - \frac{N_+}{\tau_R} \tag{11a}$$

$$\frac{\mathrm{d}N_-}{\mathrm{d}t} = \frac{(1+p)N_+}{T_s} - \frac{pN_-}{T_s} - \frac{N_-}{\tau_R} \tag{11b}$$

$$\rho\Delta\nu\frac{\mathrm{d}p}{\mathrm{d}t}=\frac{(1+p)N_+}{T_s}-\frac{pN_-}{T_s}-\frac{\rho\Delta\nu(p-p_0)}{\tau_p} \tag{11c}$$

in which $p_0=[\exp(\delta/k_BT_0)-1]^{-1}$ denotes the value of p in thermal equilibrium, and $T_s=(CH^5\cos^3\theta\sin^2\theta)^{-1}$ is the spontaneous direct relaxation time. In the last term of equation (11*c*) the phonon loss from the excited zone is incorporated as a linear term. As the phonon reabsorption is marginal in our experiments, the time constant τ_p equals, to a good approximation, the average time associated with ballistic flight out of the zone, or $\tau_p\sim L/v\approx 0.1$ ns, where L is the film thickness and v the velocity of sound.

In order to solve these equations we note that, on the relevant timescale, the left-hand side of equation (11*c*) is negligible compared to all other terms in that equation. In other words, the phonon occupation is determined by the dynamical equilibrium between the phonons and the spin system apart from a correction for the phonon loss. From equation (11*c*) we then find

$$p-p_0=\frac{\sigma}{1+\sigma}\left(\frac{N_+}{\Delta N}-p_0\right) \tag{12}$$

where $\Delta N=N_--N_+$ and where we have introduced the bottlenecking parameter

$$\sigma=\frac{\Delta N\tau_p}{\rho\Delta\nu T_s}. \tag{13}$$

Inserting p from equation (12) into equation (11*a*) and equation (11*b*), noting that $T_s=T_{\bar{E},d}(1+2p_0)$, and writing

$$N_+^0=\frac{p_0}{1+2p_0}N^* \tag{14}$$

for the time-dependent thermal equilibrium population, we find

$$\frac{\mathrm{d}N_+}{\mathrm{d}t}=-\frac{N_+-N_+^0}{(1+\sigma)T_{\bar{E},d}}-\frac{N_+}{\tau_R} \tag{15}$$

and a similar expression for N_-.

The solving of equation (15) is complicated by the the fact that $N_\pm$, and therefore σ, vary during the decay. As a consequence, the relaxation within $\bar{E}(^2\mathrm{E})$ is, strictly speaking, non-exponential. In our experiments, σ typically varies by a factor of 2 during the relaxation, but the bottlenecking contributes only a fractional correction to the relaxation time ($\sigma\lesssim 0.3$, and, more typically, <0.1). Therefore, we approximate σ by the constant value

$$\sigma_0=\frac{N^*(0)}{1+2p_0}\frac{\tau_p}{\rho\Delta\nu T_s} \tag{16}$$

which would be exact if the populations of the $\bar{E}(^2\mathrm{E})$ levels had already returned to thermal equilibrium at $t=0$. It is noted that this result is also obtained by linearization of equation (15) to first order in N_+. With the identification $T_{\bar{E}}=(1+\sigma_0)T_{\bar{E},d}$, the solution of equation (15) does indeed take on the form of equation (10). As for the dependence of $T_{\bar{E}}$ on H and θ, we recall that $T_s=T_{\bar{E},d}(1+2p_0)$, and that $1+2p_0=\coth(\delta/2k_BT_0)$ as well as ρ depend on these quantities only through δ. This finally yields

$$T_{\bar{E}}=T_{\bar{E},d}+\frac{C'}{[\delta\coth(\delta/2k_BT_0)]^2} \tag{17}$$

in which C' is an additional fitting parameter.

4.4. Results

Fits of equation (17) faithfully account for the data of T_E in figures 6 and 7. The resultant fitted parameters are $C = 62 \pm 3\ \mathrm{T^{-5}\ s^{-1}}$ and $C' = (16 \pm 3) \times 10^{-5}\ (\mathrm{cm^{-1}})^2\ \mathrm{s}$. The error in C arises mainly from the uncertainty of the temperature $T_0 \approx 1.8$ K. The result for C' is determined predominantly by the data of figure 6, since the corrections for bottlenecking in figure 7 are almost negligible. The value for C is slightly higher than that found in [6].

From C' we find $\Delta\nu \sim 0.025\ \mathrm{cm^{-1}}$ for the full width of the direct transition. This is an order of magnitude larger than the width in 700 at.ppm ruby, which originates from supertransferred hyperfine interaction with surrounding ^{27}Al nuclei, and amounts to $0.002\ \mathrm{cm^{-1}}$ [5]. It is of interest to note that the disparity can be understood in part by considering the effects of weak exchange coupling between distant Cr^{3+} ions. The exchange interaction contributes to the Zeeman splitting between the $\bar{E}(^2\mathrm{E})$ levels in either direction. In 1 at.% ruby, convolution of the distribution D_J of exchange-induced splittings [3, 12] with a Lorentzian lineshape with full width at half maximum $0.002\ \mathrm{cm^{-1}}$ broadens the line to $0.013\ \mathrm{cm^{-1}}$, which is indeed of the order of $\Delta\nu$. In 700 at.ppm ruby this effect is negligible due to the strong peaking of the D_J distribution around $J = 0$.

5. Conclusions

We have demonstrated that well orientated crystalline ruby films of submicron thickness can be grown on sapphire substrates and used in the study of acoustic phonons in restricted geometries. First of all, it has been shown that $29\ \mathrm{cm^{-1}}$ phonons can be trapped in optically excited zones within the films and their dynamics studied by conventional optical detection. Residual optically excited Cr^{3+} ions in the sapphire substrate were exploited to feed $29\ \mathrm{cm^{-1}}$ phonons from a heat pulse into the ruby film. Secondly, the direct transition between the Zeeman components of $\bar{E}(^2\mathrm{E})$ has been found to show essentially the same dependences on the magnitude and orientation of an applied magnetic field as it showed in bulk ruby. This makes it possible to use the $\bar{E}(^2\mathrm{E})$ system as a tunable detector of phonons of lower frequencies (~ 1–$5\ \mathrm{cm^{-1}}$), with the submicron typical dimension providing exceptional spatial resolution and diminishing trapping of the resonant phonons.

Acknowledgments

The authors thank G J Dirksen for invaluable assistance with the sample preparation. The work was supported by the Netherlands Foundation 'Fundamenteel Onderzoek der Materie (FOM)' and the 'Nederlandse Organisatie voor Wetenschappelijk Onderzoek (NWO)'.

References

[1] Basun S A, Kaplyanskii A A, Feofilov S P and Shekтman V L 1983 *Fiz. Tverd. Tela* **25** 2731 (Engl. Transl. 1983 *Sov. Phys.-Solid State* **25** 1570)

[2] Meltzer R S, Rives J E and Egbert W C 1982 *Phys. Rev.* B **25** 3026

[3] Goossens R J G, Dijkhuis J I and de Wijn H W 1985 *Phys. Rev.* B **32** 7065
[4] van Wijk R J, Dijkhuis J I and de Wijn H W 1991 *Phys. Rev.* B at press
[5] Geschwind S, Devlin G E, Cohen R L and Chinn S R 1965 *Phys. Rev.* **137** A1087
[6] Dijkhuis J I, Huibregtse K and de Wijn H W 1979 *Phys. Rev.* B **20** 1835
[7] van Miltenburg J G M, Jongerden G J, Dijkhuis J I and de Wijn H W 1984 *Phonon Scattering in Condensed Matter (Springer Series in Solid-State Sciences 51)* ed W Eisenmenger, K Laßmann and S Döttinger (Heidelberg: Springer) p 130
[8] Muramoto T 1973 *J. Phys. Soc. Japan* **35** 921
[9] van Dort M J, Overwijk M H F, Dijkhuis J I and de Wijn H W 1989 *Solid State Commun.* **72** 237
[10] Crank J 1975 *The Mathematics of Diffusion* 2nd edn (Oxford: Oxford University Press) p 334
[11] Blume M, Orbach R, Kiel A and Geschwind S 1965 *Phys. Rev.* **139** A314
[12] Lyo S K 1971 *Phys. Rev.* B **3** 3331